

# **Microwave Observations and Modeling of $O_2(^1\Delta_g)$ and $O_3$ Diurnal Variation in the Mesosphere**

Brad J. Sandor,<sup>1</sup> H. Clancy,<sup>2</sup> David W. Rusch,<sup>3</sup> Cora E. Randall,<sup>3</sup>  
Richard S. Eckman,<sup>4</sup> David S. Siskind,<sup>5</sup> and Duane O. Muhleman,<sup>6</sup>

Received \_\_\_\_\_; accepted \_\_\_\_\_

Short title:  $O_2(^1\Delta_g)$  FROM MICROWAVE EMISSION SPECTRA

<sup>1</sup>Jet Propulsion Laboratory, California Institute of Technology, Pasadena

<sup>2</sup>Space Science Institute, Boulder, Colorado

<sup>3</sup>Laboratory for Atmospheric and Space Physics, University of Colorado, Boulder

<sup>4</sup>NASA Langley Research Center, Hampton, Virginia

<sup>5</sup>Naval Research Laboratory, Washington, D.C.

<sup>6</sup>Division of Geology and Planetary Sciences, California Institute of Technology,  
Pasadena

**Abstract.** The first microwave measurements of an electronically excited molecular species in the earth's atmosphere are presented. Local thermodynamic equilibrium (LTE) rotational line emission from mesospheric  $O_2(^1\Delta_g)$  was observed at a frequency of 255.01794 GHz ( $\lambda \sim 1.2$  mm), employing the National Radio Astronomy Observatory NRAO millimeter facility at Kitt Peak, Arizona (32°N, 111°W). The pressure broadened line shapes of the  $O_2(^1\Delta_g)$  spectra, which were obtained in January and April of 1992 and in January and November of 1993, are inverted to retrieve  $O_2(^1\Delta_g)$  mixing profiles over the 50-70 km altitude region. The observed daytime abundances exceed ozone abundances in the lower mesosphere, which are separately retrieved with coincident  $O_3$  spectral line (249.7886 GHz) observations. The January and November 1993 observations are binned into 20-60 minute time intervals to study  $O_2(^1\Delta_g)$  diurnal behavior. Derived abundances of  $O_2(^1\Delta_g)$  between 50 and 70 km for the four observation dates are respectively 9%, 31%, 3%, and 26%, each  $\pm 10\%$ , higher than predicted, based on the simple photochemistry of lower mesospheric  $O_2(^1\Delta_g)$ . Modeled variation of  $[O_2(^1\Delta_g)]$  with time of day agrees with observed variation, in that the observed difference between model and data abundances is constant throughout the daylight hours of each observation date. Model underprediction of  $[O_2(^1\Delta_g)]$  is consistent with similar model underprediction of mesospheric  $[O_3]$

$O_2(^1\Delta_g)$  abundances derived from these 20 min observations are compared with the  $[O_2(^1\Delta_g)]$  values derived from SMF observations of the 1.27 micron emission and are discussed in the context of mesospheric  $O_3$  and HO<sub>x</sub> chemistry, and of the recent controversy over the  $O_2(^1\Delta_g)$  radiative lifetime.

## 1. Introduction

Photolysis of ozone by ultraviolet solar flux leads to large abundances (ppmv) in the upper stratosphere and mesosphere of molecular oxygen in its first electronically excited state,  $O_2(^1\Delta_g)$ . 1.27  $\mu\text{m}$  emission from  $O_2(^1\Delta_g)$  as it decays to the ground state,  $O_2(^3\Sigma_g^-)$ , has been observed from aircraft [Noxon and Vallance-Jones, 1962], balloons [Evans *et al.*, 1968; Weeks *et al.*, 1978], from satellite [Thomas *et al.*, 1984 who give a detailed history of prior 1.27  $\mu\text{m}$  airglow observations], and from the ground [Pudleton *et al.*, 1996].

$O_2(^1\Delta_g)$  mixing ratios may be inferred from measured 1.27  $\mu\text{m}$  fluxes.  $O_3$  mixing ratios may in turn be inferred from  $O_2(^1\Delta_g)$  abundances, with use of a simple photochemical modeling scheme discussed in the following section. Remote observations of 1.27  $\mu\text{m}$  emission from  $O_2(^1\Delta_g)$  have proved important for satellite measurements of mesospheric  $O_3$ . In the 70-100 km altitude region, 1.27  $\mu\text{m}$  emission from  $O_2(^1\Delta_g)$  supports the only existing technique for remote measurements of ozone. Hence, it is of considerable interest to improve our understanding of  $O_2(^1\Delta_g)$  photochemistry.

To date, infrared observations of  $O_2(^1\Delta_g)$  radiative decay have provided the only means for measuring  $O_2(^1\Delta_g)$  atmospheric abundances. A new method for making these measurements, by observation of microwave emission due to a rotational transition of the  $O_2(^1\Delta_g)$  molecule, was first reported by Clancy *et al.* [1993]. Microwave spectra of middle atmospheric constituents from ground-based observations can be inverted to provide constituent mixing profiles with one-to-two scale height vertical resolution, due to the pressure broadened line shapes of the spectral emission [Clancy and Muhleman, 1993]. Furthermore, the emission is relatively temperature insensitive (often linear), unaffected by scattering, and indicative of LTE conditions. The  $O_2(^1\Delta_g)$  and  $O_3$  molecular species exhibit reasonably strong rotational line transitions at 255.01794 and 249.7886 GHz, respectively, which provide for a unique study of  $O_2(^1\Delta_g)$  in the lower mesosphere.

The following presents an analysis of microwave spectral line observations of daytime mesospheric  $O_2(^1\Delta_g)$  and  $O_3$  within the 40-70 km altitude region. Work discussed

below represents a significant advance over the *Changy et al.*, 1993 report for the following reasons: (1) The data set has been considerably expanded. Observations discussed below were made in January 1992, April 1992, January 1993, and November 1993. (2) Improved S/N allows two of these data sets to be analyzed for  $O_2(^1\Delta_g)$  diurnal variability. (3) Improvements to the microwave instrument calibration have been made. (4) Comparisons between observed and theoretical mixing ratios have been facilitated by use of an improved photochemical model.

Microwave  $O_2(^1\Delta_g)$  observations provide a unique perspective on the current controversy over the  $O_2(^1\Delta_g)$  1.27  $\mu\text{m}$  radiative lifetime, which is of central importance to mesospheric and stratospheric ozone measurements. The 1.27  $\mu\text{m}$  radiative lifetime had long been accepted as 3880 seconds, based on the laboratory work of *Badger et al.* [1965]. Recently, the laboratory measurement of *Hsu et al.* [1992] has been interpreted by *Mlynczak and Nesbitt* [1995] to be 6800 seconds, a 75% increase. All measurements of  $O_2(^1\Delta_g)$  abundance, and hence of  $O_3$  abundance, based on 1.27  $\mu\text{m}$  observations are dependent on this laboratory determined lifetime. Thus the *Mlynczak and Nesbitt* [1995] result, if correct, would call for a major reassessment and revision of all ozone measurements derived from 1.27  $\mu\text{m}$  observations. Independent determinations of the  $O_2(^1\Delta_g)$  radiative lifetime based on decay of 1.27  $\mu\text{m}$  emission from the aurora [*Gallinger and Vallance-Jones*, 1973] and from the upper mesosphere in the evening twilight [*Pendleton et al.*, 1996] support the *Badger et al.* [1965] 3880 second lifetime.

Measurements of  $O_2(^1\Delta_g)$  mixing ratios derived from the 255 GHz observations presented below are insensitive to the 1.27  $\mu\text{m}$  radiative lifetime. For that reason, we are able to address this important issue. The 1.27  $\mu\text{m}$  volume emission rates calculated from our microwave-determined  $O_2(^1\Delta_g)$  abundances will match observed 1.27  $\mu\text{m}$  volume emission rates only if the correct radiative lifetime is used in the calculation. It is shown below that our microwave observations are consistent with the *Badger et al.* [1965] determination, and not with the *Mlynczak and Nesbitt* [1995] lifetime.

## 2. $O_2(^1\Delta_g)$ Photochemistry

There are three important  $O_2(^1\Delta_g)$  production reactions in the upper stratosphere and lower mesosphere. Solar UV photolysis of ozone:



produces  $O_2(^1\Delta_g)$  directly, where  $f$  is the production efficiency of the excited states and is  $\sim 0.9$  [Parrish *et al.*, 978]. The atomic  $O(^1D)$  photolysis product provides an indirect ( $\sim 10$ -20% below 80 km [Mlynczak and Olander, 1995]) source for  $O_2(^1\Delta_g)$  through production of  $O(^1D)$ :



laboratory uncertainties for this reaction are such that ground-state  $O_2$  rather than  $O_2(^1S)$  may result (reaction  $\theta$  between 0 and 45% of the time [Lee and Slanger, 978].

The  $O_2(^1S)$  state is collisionally deactivated to  $O_2(^1\Delta_g)$  with nearly 100% efficiency [Ogryzlo and Thrush, 974; see discussion by Mlynczak *et al.*, 993].



Radiative relaxation of  $O_2(^1S)$  to the ground state is important only above 90 km. The  $O(^1D)$  may also be quenched by reaction with  $N_2$ .

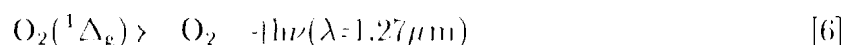


The third source for  $O_2(^1\Delta_g)$  is the direct excitation by 762 nm solar photons of  $O_2(^1S)$  to  $O_2(^1\Delta_g)$ :



followed by reaction 3. The above chemistry does not include the additional sources of  $O_2(^1\Delta_g)$  production following from  $O_2$  photolysis, which are of  $\leq 1\%$  importance below 70 km [Mlynczak *et al.*, 1993].

$O_2(^1\Delta_g)$  has two important loss processes. The molecular  $O_2(^1\Delta_g)$  specie is returned to ground state molecular oxygen either through radiative relaxation,



or collisional de-excitation,



Quenching by species other than  $O_2$  is not significant. At altitudes below 70 km, the timescale for reaction [7] is shorter than the radiative decay timescale [3880 seconds, Badger *et al.*, 1965] of reaction [6], such that collisional de-excitation dominates the loss of  $O_2(^1\Delta_g)$ . Reactions [1]-[7] account for all important production and loss of  $O_2(^1\Delta_g)$  below 70 km. For completeness, however, all the reactions listed in table 1 (adapted from the  $O_2(^1\Delta_g)$  chemistry of Mlynczak *et al.* [1993]) are included in modeling of our  $O_2(^1\Delta_g)$  observations. Inclusion of all the reactions in table 1 accounts for  $O_2(^1\Delta_g)$  production and loss to altitudes as high as 90 km, well above the 82 km upper limit of the photochemical model used here. All significant  $O_2(^1\Delta_g)$  production below 70 km follows from  $O_3$  photolysis or 762 nm excitation of  $O_2$  to  $O_2(^1\Sigma)$  (reaction 5). The relative importance of reaction 5 can be quantified [eg Mlynczak and Olander, 1995]. Making this allowance, and allowance for  $O_2(^1\Delta_g)$  production from  $O_2$  photolysis in the upper atmosphere, the abundance of  $O_2(^1\Delta_g)$  can be estimated as a proxy for  $O_3$  abundance, as discussed in the preceding section.

The following analytic approximation to the  $O_2(^1\Delta_g)$  abundance may be derived from reactions 1-7 and 10, in table 1 under conditions of photochemical equilibrium:

$$O_2(^1\Delta_g)] = \frac{1}{\tau[O_2]} \cdot A_6(J_1, O_3) \cdot \frac{J_1[O_3]k_2[O_2]}{(k_2 + k_{10})[O_2] + k_4[N_2]} + J_5[O_2] \quad (8)$$

Equation 8 illustrates that  $O_2(^1\Delta_g)$  is produced directly from  $O_3$  photolysis, indirectly from the  $O(^1D)$  product of  $O_3$  photolysis, and indirectly from  $O_2$  absorption of 762 nm solar photons.

### 3. Observations

Observations of  $O_2(^1\Delta_g)$  at 255.01794 GHz,  $O_3$  at 249.7886 GHz, and  $^{18}O$  at 203.40752 GHz were made from Kitt Peak Arizona (32°N, 112°W), using the National Radio Astronomy Observatory (NRAO)<sup>7</sup> 12-meter radio telescope and microwave receivers. Data were collected during one to three day time periods during January 1992, April 1992, January 1993, and November 1993. Representative  $O_2(^1\Delta_g)$ ,  $O_3$ , and  $^{18}O$  spectra, obtained in April 1992, are shown in figures 1, 2, and 3, respectively.

Microwave spectra of  $O_2(^1\Delta_g)$ ,  $O_3$ , and  $H_2^{18}O$  were obtained in a frequency switched mode at fixed elevation (20° or 30°) and azimuth (270° or 90°). Details of the frequency switched observations can be found in discussion of similar NO [Clancy *et al.*, 1992] and  $O_2$ ,  $O_3$ , and  $^{18}O$  [Clancy *et al.*, 1994b] Kitt Peak measurements. During the data analysis procedure a best fit to each spectrum was found for the signal within ± 6 MHz from line center. Observed spectral brightness temperatures are roughly linearly proportional to the  $O_2(^1\Delta_g)$ ,  $O_3$ , and  $^{18}O$  abundances within the 40-70 km altitude region. The vertical profiling sensitivity of the observed line shapes is demonstrated by comparable  $HO_2$  weighting functions presented in Clancy *et al.* [1994b].

Calibration of atmospheric observations from Kitt Peak has been improved [Sandor, 1995]. Absolute calibration was established by observation of the (Zeeman split)

<sup>7</sup>The National Radio Astronomy Observatory is operated by Associated Universities, Inc., under cooperative agreement with the National Science Foundation.

233.94618 GHz line of  $^{18}\text{O}^{16}\text{O}$  with the telescope elevation at  $90^\circ$ , and comparison of the retrieved mixing ratios with the well known  $^{18}\text{O}^{16}\text{O}$  abundance [Kroopnick and Craig, 1972]. (Calibration as a function of telescope elevation angle was established using microns manual tip observation sequences of the 210.8038 and 219.7886 GHz lines of  $\text{O}_3$ , and the 230.53799 GHz line of CO).

The  $\text{O}_2(^1\Delta_g)$  line emission at 255 GHz is an electric dipole, rotational transition with Zeeman splitting, due to the small net orbital angular momentum of  $\text{O}_2(^1\Delta_g)$ , into seven equally spaced components between  $\Delta M = \pm 590$  KHz from line center. Only the center five lines (which are of mixed polarization and are equally spaced within  $\Delta M = \pm 390$  KHz of line center) contribute significantly to the signal. We detect the  $\text{O}_2(^1\Delta_g)$  line simultaneously in two orthogonal, linearly polarized receivers. The spectrum of figure 1 presents the average of the two polarizations, which leads to a blending of the two sets of Zeeman splittings. Adjacent Zeeman components of the 255 GHz  $\text{O}_2(^1\Delta_g)$  line are separated by  $\Delta\nu = 200$  KHz, which is less than the 250 KHz spectral resolution of our observations. Thus individual Zeeman line components are not evident in figure 1, but the magnetic splitting does contribute to the width of the emission line and is included in the data reduction procedure. Zeeman splitting is still distinctive in 60 KHz resolution spectra of  $\text{O}_2(^1\Delta_g)$  which were observed but are not presented in this paper. An important consequence of magnetic splitting is an increase in the width of the altitude-independent contribution to line broadening, effectively degrading the altitude resolution obtainable from an  $\text{O}_2(^1\Delta_g)$  spectrum.

The  $\text{O}_3$  and  $\text{H}_2^{18}\text{O}$  line emissions at 249 and 203 GHz, respectively, were observed to support interpretation of the  $\text{O}_2(^1\Delta_g)$  measurements. The importance of  $\text{O}_3$  in  $\text{O}_2(^1\Delta_g)$  chemistry is discussed in the preceding sections.  $\text{H}_2\text{O}$  is important as the source of ozone destroying  $\text{HO}_2$ ,  $\text{OH}$ , and  $\text{HO}$  must be specified as an input to the photochemical model discussed in the following section, where the justification for using  $\text{H}_2^{18}\text{O}$  as a proxy for  $^{18}\text{O}$  is also presented.

We perform non-linear least-squares inversions of the  $O_2(^1\Delta_g)$ ,  $O_3$ , and  $H_2^{18}O$  spectral line observations in the manner described in *Clancy et al.* [1994b]. The upper stratospheric/mesospheric temperature profile is adopted from the CHRA 86 climatology *Plamming et al.*, 1990]. We also employ the expanded Solar Mesospheric Explorer (SME) temperature climatology *Clancy et al.*, 1990a]. Pressures are calculated from the temperature profiles using the hydrostatic law. To investigate the effects of uncertainty in the temperature profiles on retrieved species abundance profiles, we inverted sample spectra for the case where temperatures at altitudes 30 km and higher were increased 5K. This temperature perturbation leads to 0%, 2% and 0% changes in inferred  $O_2(^1\Delta_g)$ ,  $O_3$ , and  $H_2O$  abundances, respectively. The spectra line frequencies and line strengths are taken from the *Poynter and Pickett* [1985] line catalog. Pressure broadened line width for the 249 G  $\approx O_3$  line (2.39 MHz/mbar) is adopted from the TTRAN92 database [*Rothman et al.*, 1992], which specifies an uncertainty of  $\pm 5$ -10% in this parameter. The  $\pm 8\%$  uncertainty we use for error analysis corresponds to a  $\pm 15\%$  uncertainty in derived  $O_3$  abundance. Pressure broadened line width for the 255 G  $\approx O_2(^1\Delta_g)$  line is estimated as .8 MHz/mbar, based on laboratory work with similar transitions of ground state  $C_2$  *Liche et al.*, 1992]. We estimate our uncertainty in this parameter as  $\pm 15\%$ , which corresponds to a  $\pm 8\%$  uncertainty in derived  $O_2(^1\Delta_g)$  abundance. For the 203 G Hz line of  $H_2^{18}O$  the pressure broadened line width used is 2.7 MHz/mbar [*Rothman et al.*, 1992], and a  $\pm 20\%$  uncertainty in this value is assumed. This  $\pm 20\%$  uncertainty implies a 8% uncertainty in retrieved water abundance.

The largest uncertainty associated with  $O_3$  observations is that of collisional line width. For  $O_2(^1\Delta_g)$  observations, the 1-sigma s/n uncertainty may be comparable to collisional line width uncertainty. Table 2 provides a list of uncertainties in retrieved mixing ratios of  $O_3$ ,  $O_2(^1\Delta_g)$ , and  $H_2O$  that follow from uncertainty in the collisional line broadening coefficient for the applicable observation frequency, from uncertainty in telescope calibration, from an assumed  $\pm 5$  K uncertainty in the atmospheric temperature

profile, and from the one sigma s/n uncertainty of these observations.

The profile inversion analysis indicates that 1-3 layers over the 40-70 km altitude region are constrained by the  $O_2(^1\Delta_g)$  and  $O_3$  spectra. One layer (40-58 and 58-70 km) solutions for the  $O_3$  mixing profiles. One layer (50-70 km) or two layer (50-60 and 60-70 km) solutions for the  $O_2(^1\Delta_g)$  mixing ratios are presented, where the number of  $O_2(^1\Delta_g)$  solution layers derived from a given 255 GHz spectrum is controlled by the noise level of the observation. Mixing profiles are constrained to vary smoothly across layer boundaries. The inversions do not resolve vertical variations in the  $O_3$  and  $O_2(^1\Delta_g)$  mixing profiles finer than these solution layer widths. The small contributions of  $O_3$  and  $O_2(^1\Delta_g)$  emission above and below these layers are calculated from a priori  $O_3$  and  $O_2(^1\Delta_g)$  mixing profiles, which are constrained to blend smoothly to the mixing profile solutions.

Retrieved altitude profiles of  $O_2(^1\Delta_g)$  mixing ratios for the four observation dates are shown in figure 4. Each profile represents the full day observation. Times of day represented in figure 4 and table 3 are 11am-5pm for January 19 and 21, 1992, 1:30-2:30 pm for April 10, 1992, 3:10-5:10 pm for January 24, 1993, and 8:45am-4pm for November 29 and 30, 1993. For the model vs data comparisons in table 3, model  $O_2(^1\Delta_g)$  abundances were averaged over the times of day corresponding to the observations. The single error bars on each of the January and April 1992  $O_2(^1\Delta_g)$  altitude profiles represent retrieval uncertainty for a 50-70 km altitude layer. The two error bars on each of the January and November 1993  $O_2(^1\Delta_g)$  altitude profiles represent retrieval uncertainties for 50-60 and 60-70 km altitude bins, where this higher altitude resolution follows from the higher s/n of the 1993 observations.

Altitude profiles of  $H_2O$  mixing ratios, derived from the  $H_2^{18}O$  observations, for the four observation dates are shown in figure 5. Error bars correspond to s/n uncertainties in the retrieved profiles for altitude bins 46-58 and 58-70 km. Each profile represents the full day observation; details of each observation and comparison with other water

profile data for each date are listed in table 5. Water vapor profiles measured from Kitt Peak compare favorably with coincident measurements made with the Microwave Limb Sounder (MLS) 183 GHz radiometer [Lahoz, 1991] on the Upper Atmospheric Research Satellite (UARS), and with ground-based 22.2 GHz measurements [Nedoluha *et al.*, 1995] made from the Table Mountain, California (34.4° N, 117.7° W) facility 650 km from Kitt Peak.

Figure 6 shows a sample retrieved O<sub>3</sub> altitude profile, along with the corresponding 4-year monthly zonal mean O<sub>3</sub> abundances derived from observations of the SME UV [Rusch *et al.*, 1983] and IR (1.27 micron) [Thomas *et al.*, 1984] instruments. Photochemical model O<sub>3</sub> profiles, discussed in the following section, are also presented in figure 6.

Observational parameters for the four observation dates are summarized for each species in tables 3-5. System temperatures for the O<sub>2</sub>(<sup>1</sup>Δ<sub>g</sub>) integrations reflect that the the ordering of observation dates from lowest to highest noise is: January 1993, November 1993, April 1992, January 1992. For the January and November 1993 observations, s/n was sufficiently high that O<sub>2</sub>(<sup>1</sup>Δ<sub>g</sub>) abundances could be retrieved from numerous 20-90 minute 255 GHz integrations. These data enable analysis of diurnal O<sub>2</sub>(<sup>1</sup>Δ<sub>g</sub>) diurnal behavior, discussed in detail below. A similar diurnal study of O<sub>3</sub> from short 249 GHz integrations was conducted for January, 1993.

#### 4. Photochemical Model

As part of the data interpretation, a one dimensional photochemical model [Siskind *et al.*, 1995] was used to calculate theoretical abundances of chemical species as a function of time of day. This model, an updated version of that used by Rusch and Eckman [1985], calculates species abundances for altitudes 36-82 km. Improvements to O<sub>3</sub> photochemistry in this model include the use of spherical ray tracing at twilight, a partial relaxation of the odd-oxygen family approximation, and a scattering correction to O<sub>3</sub>

photolysis.

Species with photochemical lifetimes sufficiently long that horizontal transport is important are specified as model inputs. The key such long-lived species for this study is water, and the input profile used is derived from the 203 GHz  $\text{H}_2^{18}\text{O}$  observations described above by [Miyoshi et al. \(2003\)](#), the standard mean ocean water (SMOW) value of  $[\text{H}_2^{18}\text{O}]/[\text{H}_2^{16}\text{O}]$  [Kaye, 1987]. The atmospheric ratio  $[\text{H}_2^{18}\text{O}]/[\text{H}_2^{16}\text{O}]$  was observed by [Rinsland et al. \(1991\)](#) to match the SMOW ratio up to 54 km, the top of their measurement range. Model  $\text{O}_3$  abundance roughly scales as  $[\text{H}_2^{16}\text{O}]^{1/2}$  [Clancy et al., 1994b], so the  $\sim \pm 20\%$  uncertainty in measured water vapor corresponds to a  $\sim \pm 10\%$  uncertainty in model ozone. Because  $\text{O}_3$  photolysis is the dominant source of  $\text{O}_2(^1\Delta_g)$ , uncertainty in retrieved water vapor abundance similarly translates into a model  $[\text{O}_2(^1\Delta_g)]$  uncertainty of  $\sim \pm 10\%$ . This square root dependence of  $[\text{O}_3]$  and  $[\text{O}_2(^1\Delta_g)]$  on water is seen in comparison of model runs with different water inputs, discussed below.

The standard version of this model includes some 50 photochemical reactions. For work presented here the reactions specifically relevant to  $\text{O}_2(^1\Delta_g)$  chemistry (table 1), not already included have been adapted from [Mlynczak et al. \(1993\)](#) and added to the Eckman-Siskind model.

The standard model was run with reaction rates from the JPL 1994 compilation [DeMore et al., 1994]. Altered versions of the standard model were run by perturbing reaction rates away from their JPL 1994 values. The perturbed model version discussed most extensively in the following section differs from the standard model in that it uses a rate coefficient for  $\text{HO}_2 + \text{O} \rightarrow \text{O}_2 + \text{O}_2$  reduced 40% (twice the quoted uncertainty) from the standard JPL 1994 value [DeMore et al., 1994].

## 5. Results and Discussion

### 5.1. Model-Data Comparisons

Observed 50-70 km full-day  $O_2(^1\Delta_g)$  abundances are higher than model values by 9, 31, 3, and 26 %, for an average over the four observation periods of 17% (table 3). The high  $s/n$  spectra obtained in January and November 1993 allow better ( $\sim 10$  km) altitude resolution for those dates. In figure 4, the single error bar on each of the January and April 1992 altitude profiles indicates retrieval for a single, 50-70 km layer; the two ("1101" bars on each of the January and November 1993 profiles indicate retrieval for two layers (50-60 and 60-70 km). The shape of the retrieved January profile is well matched by the shape of the standard photochemical model. The two layer retrieved November profile, however, is enhanced  $\sim 50 \pm 10\%$  over the model for 50-60 km, and  $\sim 10 \pm 10\%$  over the model for 60-70 km. This difference in shape of the November 1993 retrieved and model  $[O_2(^1\Delta_g)]$  profiles is not affected by any of the changes to the photochemical model discussed below.

As an alternative to obtaining 10 km altitude resolution with the January and November 1993  $O_2(^1\Delta_g)$  observations, the single 50-70 km altitude bin may be used with the full-day observations broken into much shorter intervals. 20-35 minute temporal resolution was obtained from the January 24, 1993  $O_2(^1\Delta_g)$  observation and a diurnal analysis performed for the local solar time range 3:10-6:20 pm. Similarly, 30-90 minute resolution was obtained for 8:45 am to 4:00 pm from the November 29-30, 1993  $O_2(^1\Delta_g)$  observation; data from two consecutive days were combined to obtain improved  $s/n$  and were analyzed as a single diurnal period. Figures 7 and 8 illustrate that photochemical model  $O_2(^1\Delta_g)$  diurnal behavior agrees with the observations. Horizontal error bars indicate the length of each observation, and vertical error bars indicate uncertainty in the retrieved 50-70 km mixing ratios. The shapes of the  $O_2(^1\Delta_g)$  mixing ratio vs time of day curves are the same for the data and model. The data/model offsets are roughly

constant through the day, and are consistent with the full-day data/model differences listed in table 3.

Table 4 summarizes retrieved daytime  $O_3$  values from the four observation periods, where only daytime results are reported in order to facilitate comparison with the (daytime) SME climatologies. Eleven 249 GHz  $O_3$  observations were made January 23-25, 1993. Mixing ratios derived from these data are plotted vs time of day for a single diurnal period and at three altitudes in figures 9, 10, and 11. Horizontal error bars on the data points indicate the length of each observation (6 or 12 minutes). Vertical error bars indicate uncertainty in derived mixing ratio. Mixing ratio uncertainties are dominated by the effect of an 8% uncertainty in the collisional broadening coefficient. Uncertainty due to noise in these strong-signal observations is small, and this is reflected by the small vertical scatter of the data points relative to the size of the error bars. The shapes of the  $O_3$  mixing ratio vs time of day curves are the same for the data and model. The data/model offsets are roughly constant through the day for each altitude, with the sole exception of the 8:45pm observation. Figures 9-11 illustrate that our  $O_3$  data are 15-25% under-predicted by the standard model and that the data vs model discrepancy increases with altitude. This underprediction is the ozone deficit [Solomon *et al.*, 1983; Fluszkiewicz and Allen, 1993] seen in every other comparable data set. Our  $O_3$  observations are in agreement with the SME IR [Thomas *et al.*, 1984] and UV [Rusch *et al.*, 1983] 4-year monthly zonal means.

Because  $O_3$  photolysis is the dominant source of  $O_2(^1\Delta_g)$  below 70 km, the most consistent way to interpret the model under-prediction of observed  $O_2(^1\Delta_g)$  is as a consequence of the model's under-prediction of  $O_3$ . Our  $O_2(^1\Delta_g)$  (figures 7 and 8) and  $O_3$  (figures 9-11) observations are compared with results of a perturbed photochemical model in which  $k(HO_2 + OOH) \rightarrow O_2$  is reduced 40% (i.e. to 60% the accepted 1.11, § 14 value). This perturbation is motivated by the conclusions of Clancy *et al.* [1994b], that a reduction of this rate coefficient will simultaneously improve model deficits in  $O_3$  and  $HO_2$ . It is fur-

ther motivated by more recent microwave  $\text{O}_2$  observations [Sandor and Clancy, 1996], and by satellite observations [Conway *et al.*, 1996; Summers *et al.*, 1996] of substantially less lower mesospheric OH than predicted with standard models (a model OH surplus). Also, Siskind *et al.* [1996] report a reduction in this reaction rate adequately addresses a low temperature bias in the model for  $\sim 60$ -80 km, though not a larger model cold bias at higher altitudes. That this reduction in the rate coefficient is smaller than the 60-80% reduction recommended by Clancy *et al.* [1994b] follows from use of the improved photochemical model and from the improved Kitt Peak calibration.

Model  $[\text{O}_2(^1\Delta_g)]$  is increased  $\sim 20\%$  by the 40% reduction in the rate coefficient for  $\text{C} + \text{O} \rightarrow \text{O}_2$ . This rate change provides good agreement with the observation that  $[\text{O}_2(^1\Delta_g)]$  is on average 17% higher (table 3) than the standard model prediction, and simultaneously gives much improved agreement with observed  $\text{O}_3$  (figures 9-11, table 4).

The  $\text{HO}_2 + \text{O}$  rate reduction is not a unique explanation of the  $[\text{O}_2(^1\Delta_g)]$  observations reported here, but it is the simplest explanation that also addresses model vs data discrepancies for  $\text{O}_3$  (eg. this study),  $\text{HO}_2$  [Clancy *et al.*, 1994b], and  $\text{C}$ . [Summers *et al.*, 1996]. For example, a 20% (1 sigma) reduction of the  $[\text{O}_2(^1\Delta_g)]$  collisional deactivation coefficient brings model  $[\text{O}_2(^1\Delta_g)]$  into agreement with the data, but has no effect on model  $\text{O}_3$ ,  $\text{O}_2$ , or OH. As another example, reducing the model water input by 40-50% provides good model correspondence with observed  $[\text{O}_2(^1\Delta_g)]$  and  $\text{O}_3$ . However such a 40-50% water reduction would only worsen model  $[\text{O}_2(^1\Delta_g)]$  underprediction [Clancy *et al.*, 1994b], and is unrealistic in view of the excellent agreement between our water observations and others listed in table 5.

### 5.2. $[\text{O}_2(^1\Delta_g)]$ 1.27 $\mu\text{m}$ Radiative Lifetime

An accurate value for the  $[\text{O}_2(^1\Delta_g)]$  1.27 $\mu\text{m}$  radiative lifetime (the reciprocal of the Einstein A value) is required for interpreting observed 1.27 $\mu\text{m}$  volume emission rates

in terms  $O_2(^1\Delta_g)$ , and hence  $O_3$ , abundances. The value  $\Lambda = 2.6 \times 10^{-4} \text{ s}^{-1}$  determined by *Badger et al* [1965] had long been accepted as accurate. More recently, *Mlynczak and Ncsbill* [1995] have interpreted the *Hsu et al* [1992] laboratory measurement of the Einstein B value for absorption of 1.27 micron photons by  $O_2(^1\Delta_g)$  to imply an  $O_2(^1\Delta_g)$  Einstein A value of  $1.5 \times 10^{-4} \text{ s}^{-1}$ . This is 42% smaller than the previously accepted value  $2.6 \times 10^{-4} \text{ s}^{-1}$  [Badger et al., 1965], and if this new rate is correct a re-analysis of all mesospheric ozone measurements based on 1.27 micron remote observations is called for. *Mlynczak and Ncsbill* [1995], using the  $\Lambda = 1.5 \times 10^{-4} \text{ s}^{-1}$  value, have reinterpreted the SME 1.27 micron volume emission rates to imply ozone densities  $\sim 75\%$  higher than inferred by *Thomas et al.* [1997] in the region below 70 km, where  $O_2(^1\Delta_g)$  loss is dominated by collisions with ground state  $O_2$ .

Ground-based observations of the decay of 1.27  $\mu\text{m}$  emission from auroral displays [eg *Gallinger and Vallance*, 1973] imply a lifetime of about an hour, consistent with the *Badger et al.* [1965] A value, which corresponds to a 64 minute lifetime. Ground-based observations of 1.27  $\mu\text{m}$  emission decay from the upper mesosphere in the evening twilight [*Pendleton et al.*, 1996] indicate a lifetime of 44 to 61 minutes, also consistent with *Badger et al.* [1965], and much shorter than the *Mlynczak and Ncsbill* [1995] lifetime of 110 minutes.

In contrast to inferences from 1.27 micron data,  $O_2(^1\Delta_g)$  abundances derived from the 1.2 mm observations described in this paper are independent of the Einstein A value in the (collisionally dominated) altitude regime below 70 km. However, 1.27 micron volume emission rates are easily calculated from these 1.2 mm  $O_2(^1\Delta_g)$  abundances for any assumed A value, and will match observed 1.27 micron volume emission rates only for use of the correct A value. Thus the 1.2 mm observations presented in this paper provide a test of the laboratory determined Einstein A's fundamentally different than the tests allowed by 1.27 micron observations.

Altitude profiles of the  $O_2(^1\Delta_g)$  1.27 micron volume emission rate are shown in

figure 12. Values observed with SME on March 1, 1983, have been adopted from figure 8 of *Thomas et al.* [1984]. Diamonds and triangles indicate the SME results at 44°N and 10°N latitude, respectively, bracketing the 32°N latitude of Kitt Peak. Volume emission rates corresponding to our 1.2 mm observations are simply  $[O_2(^1\Delta_g)] \times A$ , and are shown by the solid and dotted curves for the Einstein A values  $2.6 \times 10^{-4}$  [Badger *et al.*, 1965] and  $1.5 \times 10^{-4}$  [Mlynczak and Nesbitt, 1995], respectively, with one solid and one dotted curve for each observation date. Error bars on the solid and dotted curves correspond to the uncertainties in  $O_2(^1\Delta_g)$  abundances derived from the 1.2 mm observations. Altitude profiles with one error bar represent one layer (January and April, 1992) retrievals. Altitude profiles with two error bars represent two layer (January and November, 1993) retrievals.

For all four observation dates, the 1.27 micron volume emission rates corresponding to our 1.2 mm  $O_2(^1\Delta_g)$  measurements are in close agreement with the observed [Thomas *et al.*, 1984] 1.27 micron volume emission rates for an Einstein A value  $2.6 \times 10^{-4}$  [Badger *et al.*, 1965], but not for  $A = 1.5 \times 10^{-4}$  [Mlynczak and Nesbitt, 1995]. This is strong evidence that the *Badger et al.* [1965] A value is correct and that the *Mlynczak and Nesbitt* [1995] A value is in error. We do not know the reason for this error. However, we find no problem with the analysis of *Mlynczak and Nesbitt* [1995], and therefore speculate the most likely source of the *Mlynczak and Nesbitt* [1995] error is an error in the *Hsu et al.* [1992] measurement of the Einstein B value.

## 5. Summary

The first microwave observation of an electronically excited molecular species in Earth's atmosphere was made in January 1992 with observation of the 255 GHz emission of  $O_2(^1\Delta_g)$ . Subsequent, higher signal to noise, 255 GHz  $O_2(^1\Delta_g)$  observations were made in April 1992, January 1993, and November 1993. One layer (50-70 km) daytime retrieved  $O_2(^1\Delta_g)$  abundances derived from these observations are  $3-31 \pm 10\%$  higher than

abundances predicted with a standard photochemical model. The average of the 50–70 km  $[\text{O}_2(^1\Delta_g)]_{\text{obs}}/[\text{O}_2(^1\Delta_g)]_{\text{model}}$  ratios from the four observation dates is 1.17. This 17% average enhancement of observed over model  $\text{O}_2(^1\Delta_g)$  is well matched by running the model with a 40% reduction in the rate coefficient for  $\text{HO}_2 + \text{O} \rightarrow \text{O}_2 + \text{OH}$ . Variability of the enhancement between observation dates is not addressed by the rate change. This model perturbation also substantially improves agreement between model and observed  $\text{O}_3$ , addressing the long-standing problem of a middle atmosphere ozone deficit [Solomon *et al.*, 1983; Fluszkiewicz and Allen, 1993], and is consistent with lower mesospheric model vs data discrepancies reported elsewhere for  $\text{HO}_2$  [Clancy *et al.*, 1994], OH [Summers *et al.*, 1996], and temperature [Siskind *et al.*, 1996].

Improved altitude resolution was obtained with two layer (50–60 and 60–70 km) data inversions for high-s/n observations made in January and November, 1993. The shape of the retrieved January profile is well matched by the shape of the standard photochemical model. The two layer November profile has significantly more enhancement of observed over model  $[\text{O}_2(^1\Delta_g)]$  in the 50–60 than in the 60–70 km altitude bin.

Shorter integration time  $\text{O}_2(^1\Delta_g)$  1993 observations for both January and November have been analyzed for diurnal variability. For January 1993, an extensive diurnal analysis was also done with  $\text{O}_3$  observations. For both  $\text{O}_2(^1\Delta_g)$  and  $\text{O}_3$  there is agreement between observed behavior and the shape of the species abundance vs time of day model curves. That is, the enhancements of  $[\text{O}_2(^1\Delta_g)]$  listed in table 3 hold at all observation times of day.

In general, these microwave  $\text{O}_2(^1\Delta_g)$  observations are an important confirmation of the utility of 1.27 micron observations of  $\text{O}_2(^1\Delta_g)$  as a proxy for mesospheric ozone. The consistency between model deficits of  $\text{O}_2(^1\Delta_g)$  and  $\text{O}_3$  implies that  $\text{O}_2(^1\Delta_g)$  chemistry is well understood. Addressing a more specific issue, microwave  $\text{O}_2(^1\Delta_g)$  observations provide a new argument that the 1.27 micron radiative lifetime determination of Badger *et al.* [1965], which is crucial to mesospheric  $\text{O}_3$  studies, is not in error.

**Acknowledgments.** We gratefully acknowledge the assistance of NRAO staff at Kitt Peak.

In particular, we thank Phil Jewell for his constant technical support of our observations and NRAO telescope operators Lisa Ehgel, Paul Hart, Harry Stahl, and Ed Treiber for their invaluable operational support. We also thank Mary Mlynarz and Susan Solomon for helpful discussions. J. Sander gratefully acknowledges support from the Resident Research Associateship program of the National Research Council. The work at the Jet Propulsion Laboratory, California Institute of Technology, was sponsored by the National Aeronautics and Space Administration and the National Research Council.

## References

- Badger, R. M., A.C. Wright, and R.F. Whitlock, Absolute intensities of the discrete and continuous absorption bands of oxygen gas at 1.26 and 1.065  $\mu$  and the radiative lifetime of the  $^1\Delta_g$  state of oxygen, *J. Chem. Phys.*, **43**, 4345-4350, 1965.
- Clancy, R.T., D.W. Rusch, and J.O. Muhleman, A microwave measurement of high levels of thermospheric nitric oxide, *Geophys. Res. Lett.*, **19**, 261264, 1992.
- Clancy, R.T., and J.O. Muhleman, Ground-based microwave spectroscopy of the earth's stratosphere and mesosphere, in *Atmospheric Remote Sensing by Microwave Radiometry*, edited by M. A. Janssen, pp. 335-382, Wiley, New York, 1993.
- Clancy, R.T., B.J. Sandor, and D.W. Rusch, First measurements of the 1.2mm emission line of mesospheric  $O_2(^1\Delta_g)$ : Implications for a smaller collisional de-excitation rate coefficient for  $O_2(^1\Delta_g)$ , *Ann. N.Y. Acad. Sci.*, **74**, 169, 1993.
- Clancy, R.T., D. W. Rusch, and M.T. Callan, Temperature minima in the average thermal structure of the middle atmosphere (70-50 km) from analysis of 40- to 92  $\mu$ m SME global temperature profiles, *J. Geophys. Res.*, **99**, 19,001-19,020, 1994a.
- Clancy, R.T., B.J. Sandor, D. W. Rusch, and J.O. Muhleman, Microwave observations and modeling of  $O_3$ ,  $H_2O$ , and  $HO_2$  in the mesosphere, *J. Geophys. Res.*, **99**, 5465-5473, 1994b.
- Conway, R.R., M.H. Stevens, J. G. Cardon, S.E. Zasadil, C.M. Brown, S. Merrill, and G.H. Mount, Satellite measurements of hydroxyl in the mesosphere, Submitted to *Geophys. Res.*, **101**, 1996.
- DeMore, W. B., P. Sander, J. M. Golden, R. F. Hampson, M. J. Kurylo, C. J. Howard, A. R. Ravishankara, C. E. Kolb, and M. J. Molina, *Chemical kinetics and photochemical data for use in stratospheric modeling, in Evaluation 1, JPL Publ. 9426*, Jet Propulsion Lab., Pasadena, Calif., 1994.
- Eluszkiewicz, J., and M. Allen, A global analysis of the ozone deficit in the upper stratosphere and lower mesosphere, *J. Geophys. Res.*, **98**, 1069-1082, 1993.
- Evaus, W.F.J., D. M. Hunt, E.J. Llewellyn, and A. Vallance Jones, Altitude profile of the infrared atmospheric system of oxygen in the dayglow, *J. Geophys. Res.*, **73**, 2885, 1968.

- Fairchild, C.E., E.J. Stone, and G.M. Lawrence, Photofragment spectroscopy of ozone in the UV region 270-310 nm and at 600 nm, *J. Chem. Phys.*, **69**, 3632, 1978.
- Fleming, E.L., S. Chandra, J.J. Barnett, and M. Corney, Pressure, Zonal Wind, and Geopotential Height as Functions of Latitude, in *COSPAR International Reference Atmosphere: 1986; Part II: Middle Atmosphere Models*, edited by D. Rees, J.J. Barnett, and K. Labitzke, pp. 11-59, Pergamon Press, New York, 1990.
- Gattinger, R.L., and A. Vallance-Jones, Observation and interpretation of the O<sub>2</sub> 1.27  $\mu$ m emission enhancement in the aurora, *J. Geophys. Res.*, **78**, 8305-8313, 1973.
- Hsu, Y.P., Y. P. Lee, and J.F. Ogilvie, Intensities of lines in the band a.  $\Delta_g(\nu' = 0) - X^3\Sigma_g^-(\nu'' = 0)$  of <sup>16</sup>O<sub>2</sub> in absorption, *Spectrochimica Acta*, **48A**, 1227-1230, 1992.
- Kaye, J. A., Mechanisms and observations for isotope fractionation of molecular species in planetary atmospheres, *Rev. Geophys.*, **25**, 1609-1658, 1987.
- Kroopnick, P., and H. Craig, Atmospheric oxygen: Isotopic composition and solubility fractionation, *Science*, **175**, 54-55, 1972.
- Liebe, H.J., P. W. Rosenkranz, and G.A. Hufford, Atmospheric 60-GHz oxygen spectrum: New laboratory measurements and line parameters, *J. Quant. Spectrosc. Radiat. Transf.*, **48**, 629-643, 1992.
- Lahoz, W.A., The 183 GHz water and ozone channels on the Upper Atmospheric Research Satellite microwave limb sounder, *Int. J. Remote Sensing*, **12**, 33-53, 1991.
- Lahoz, W.A., M.R. Suttie, L. Froidevaux, R. S. Harwood, C.L. Lau, T.A. Lungu, G.E. Peckham, H.C. Pumphrey, W.G. Read, Z. Shippony, R.A. Suttie, and J.W. Waters, Validation of UARS III 1/S 183 GHz H<sub>2</sub>O and O<sub>3</sub> channels, *J. Geophys. Res.*, **101**, 10,129-10,149, 1996.
- Lee, L.C., and T.G. Slanger, Observations of O(<sup>1</sup>D -  $\gamma^3P$ ) and O<sub>2</sub>(b<sup>1</sup> $\Sigma_g^-$  -  $\gamma$  X<sup>3</sup> $\Sigma_g^-$ ) following O<sub>2</sub> photodissociation, *J. Phys. Chem.*, **69**, 4053-4060, 1978.
- Liebe, H.J., P.W. Rosenkranz, and G. A. Hufford, Atmospheric 60-GHz oxygen spectrum: New laboratory measurements and line parameters, *J. Quant. Spectrosc. Radiat. Transf.*, **48**, 629-643, 1992.
- Mlynczak, M. G., S. Solomon, and D.S. Zaras, An updated model for O<sub>2</sub>(<sup>1</sup> $\Delta_g$ ) concentrations in the mesosphere and lower thermosphere and implications for remote sensing of ozone at

- 1.27  $\mu\text{m}$ , *J. Geophys. Res.*, **98**, 18,639-18,648, 1993.
- Mlynczak, M.G., and D.J. Nesbitt, The Einstein coefficient for spontaneous emission of the  $\text{O}_2(^1\Delta_g)$  state, *Geophys. Res. Lett.*, **22**, 1381-1384, 1995.
- Mlynczak, M.G., and J. S. Olander, On the Utility of the Molecular Oxygen Dayglow Emissions as Proxies for Middle Atmospheric Ozone, *Geophys. Res. Lett.*, **22**, 1377-1380, 1995.
- Nedoluha, G.E., R.M. Bevilacqua, R.M. Gomez, D.L. Thacker, W.B. Waltman, and C. A. Pauls, Ground-based measurements of water vapor in the middle atmosphere, *J. Geophys. Res.*, **100**, 2927-2939, 1995.
- Noxon, J.F., and A. Vallance Jones, Observation of the (0,0) band of the  $\text{O}_2(^1\Delta_g)\text{-O}_2(^1\Sigma_g^-)$  systems of oxygen in the day and twilight airglow, *Nature*, **196**, 157, 1962.
- Ogryzlo, E.A., and B.A. Thrush, The vibrational excitation of  $\text{H}_2\text{O}$  and  $\text{CO}_2$  by  $\text{O}_2(^1\Sigma_g^-)$ , *Philos. Mag.*, **24**, 314-316, 1974.
- Pendleton, W.R. Jr., D.J. Baker, R.J. Reese, R.R. and O'Neil, Decay of  $\text{O}_2(^1\Delta_g)$  in the evening twilight airglow: Implications for the radiative lifetime, *Geophys. Res. Lett.*, **23**, 1013-1016, 1996.
- Poynter, R.L., and H.M. Pickett, Submillimeter, millimeter, and microwave spectral line catalog, *Appl. Opt.*, **24**, 2235-2240, 1985.
- Rinsland, C.P., M.R. Gunson, J.C. Foster, R.A. Toth, C.B. Farmer, and R. Zander, Stratospheric profiles of heavy water vapor isotopes and  $\text{CH}_3\text{D}$  from analysis of the ATMOS space lab infrared solar spectra, *J. Geophys. Res.*, **96**, 1057-1068, 1991.
- Rothman, L.S., R.R. Gamache, R.H. Tipping, C.P. Rinsland, M.A.H. Smith, J. Chris Benner, V. Malathy Devi, J.-M. Flaud, C. Camy-Peyret, A. Perrin, A. Goldman, S.T. Massie, L.R. Brown, and R.A. Toth, The HITRAN Molecular Database: Editions of 1991 and 1992, *J. Quant. Spectrosc. Radiat. Transf.*, **48**, 469-507, 1992.
- Rusch, D.W., G.H. Mount, C.A. Barth, G.J. Rottman, R.J. Thomas, G.E. Thomas, R.W. Sanders, G.M. Lawrence, and R.S. Eckman, Ozone densities in the lower mesosphere measured by a limb scanning ultraviolet spectrometer, *Geophys. Res. Lett.*, **10**, 241, 1983.
- Rusch, D.W., and R.S. Eckman, Implications of the comparison of ozone abundances measured by the Solar Mesospheric Explorer to model calculations, *J. Geophys. Res.*, **90**, 12, 9911-9988, 1998.

- 1985.
- Sandor, B.J., Microwave studies of chemistry of the middle atmosphere, Ph.D. thesis, Univ. of Colorado, Boulder, 1995.
- Sandoz, P., J.L., and G.P. Clancy (1996). Microwave observations of the diurnal variation of HO<sub>2</sub> in the mesosphere, *American Geophysical Union Spring Meeting*, Baltimore (M1).
- Siskind, D.E., B.J. Connor, R.S. Eckman, E.F. Remsburg, J.L. Tsou, and A. Parrish, An inter-comparison of model ozone deficits in the upper stratosphere and mesosphere from two data sets, *J. Geophys. Res.*, 100, 11, 19111, 201, 1995.
- Siskind, D.E., M.E. Summers, J.T. Bacmeister, and R.R. Conway (1996). On the contribution of exothermic chemistry to the thermal budget at mesopause altitudes, *American Geophysical Union Spring Meeting*, Baltimore (M1).
- Solomon, S., D.W. Collins, R.J. Thomas, and R.S. Eckman, Comparison of mesospheric ozone abundances measured by the solar mesospheric explorer and model calculations, *Geophys. Res. Lett.*, 10, 249-252, 1983.
- Summers, M. E., R.R. Conway, D.E. Siskind, R.M. Bevilacqua, D. Strobel, and S. Zasadil, Mesospheric HO<sub>x</sub> photochemistry: Constraints from recent satellite measurements of OH and H<sub>2</sub>O, Submitted to *Geophys. Res. Lett.*, 1996.
- Thomas, J.L., C. A. Barth, D. W. Rusch, and R. W. Sanders, Solar Mesosphere Explorer near-infrared spectrometer: Measurements of 1.27 μm radiances and the inference of mesospheric ozone, *J. Geophys. Res.*, 89, 9569-9580, 1984.
- Wang, J.L., R.E. Good, S. Randhawa, and M. Trinks, Ozone measurements in the stratosphere, mesosphere, and lower thermosphere during Aladdin T4, *J. Geophys. Res.*, 83, 978-982, 1978.

**Table 1.** Reactions describing  $\text{O}_2(^1\Delta_g)$  photochemistry. This list is adapted from *Mlynarczyk et al.* [1993], and reactions not already included in the Pankovian-Siskind photochemical model [Pankovian and Leckman, 1985; Siskind *et al.* 1995] were added to it.

**Table 2.** Uncertainties involved in retrieval of  $\text{O}_2(^1\Delta_g)$ ,  $\text{O}_3$ , and  $\text{H}_2^{18}\text{C}$  abundances from microwave observations

**Table 3.** Summary description of  $\text{O}_2(^1\Delta_g)$  observations and results. Ratios of model to data values are for layer (50-70 km) data retrievals. Uncertainties are the rms sum of error sources listed in table 2, and are dominated by the pressure broadening coefficient uncertainty.

**Table 4.** Summary description of  $\text{O}_3$  observations and results. Path mixing ratio derived from 249 GHz Kil Peak observations is the average of the stated number of daytime observations; the  $\pm 7\%$  errors are dominated by the pressure broadening uncertainty. SMF values are the 4-year monthly zonal means.

**Table 5.** Summary description of H<sub>2</sub>O observations and results. Values derived from Kitt Peak 203 GHz H<sub>2</sub><sup>18</sup>O spectra compare favorably with values from coincident measurements made from nearby Table Mountain, California and from UARS MLS. Table Mountain mixing ratios for April are April 1 (1992 measured values (R. Bevilacqua, personal communication, 1992), and for January 1992, January 1993, and November 1993 are the monthly average values for the months January, January, and October 1992, [Nedoluha et al., 1995]. M<sub>1</sub>/S values [1992, 1993] are from the water vapor profile measured closest to Kitt Peak on the day of the Kitt Peak water observation.

**Figure 1.** 255 GHz spectrum of O<sub>2</sub>(<sup>1</sup>Δ<sub>g</sub>), observed April 10, 1:30 - 2:30 pm, 1992. The 250 KHz resolution data are represented by the histogram. The dashed curve is the best fit to the data. The dotted curve is the synthetic emission line corresponding to the standard photochemical model O<sub>2</sub>(<sup>1</sup>Δ<sub>g</sub>) altitude profile, and illustrates that the difference between measured and model [O<sub>2</sub>(<sup>1</sup>Δ<sub>g</sub>)] is well outside the noise of the observation.

**Figure 2.** 249 GHz spectrum of  $O_3$ , observed April 10, 1:00 pm, 1992. The 250 KHz resolution data are represented by the histogram. The dashed curve is the best fit to the data, and the dotted curve is the synthetic emission line corresponding to the standard photochemical model  $O_3$  altitude profile.

**Figure 3.** 203 GHz spectrum of  $H_2^{18}O$ , observed April 10, 1992. The 250 KHz resolution data are represented by the histogram. The dashed curve is the best fit to the data.

**Figure 4.**  $O_2(^1\Delta_g)$  altitude profiles retrieved from observations on the indicated dates. Solid curve: 1-layer (50-70 km)  $O_2(^1\Delta_g)$  profile from observation January 19 (1-5 pm) and January 21 (11am-2pm), 1992. Dotted curve: 1-layer (50-70 km)  $O_2(^1\Delta_g)$  profile from observation 1:30-2:30pm April 10, 1992. See figure 1d. Dashed curve: 2-layer (50-60 and 60-70 km)  $O_2(^1\Delta_g)$  profile from observation 3:10-5:10pm January 24, 1993. Dot-dashed curve: 2-layer (50-60 and 60-70 km)  $O_2(^1\Delta_g)$  profile from observation 8:45am-12:30pm and 2-4 pm November 29 and 30, 1993. Error bars on each profile represent the rms sum of uncertainties associated with s/n, calibration, and pressure broadening.

**Figure 5** 2-layer (48-58 and 58-70 km) H<sub>2</sub>O altitude profiles retrieved from observations on the indicated dates. Solid curve: January 19 and 22, 1992. Dotted curve: April 10,1992. Dashed curve: January 23, 99; Dot-dashed curve: November 29, 1993. Error bars on each profile sigma s/1 uncertainties.

**Figure 6.** Representative O<sub>3</sub> altitude profile. The solid curve was derived from the 249 GHz data shown in figure 2d; a two layer retrieval (48-58 and 58-72 km) was done. Error bars indicate precise broadening, calibration, and 1-sigma s/n uncertainties. The dashed line is the standard photochemical model result, corresponding to the dotted line spectrum in figure 2d. The dotted line is the photochemical model result with the indicated rate change. Also shown are the 4-year monthly mean values derived from SMI IR and UV observations.

**Figure 7.**  $O_2(^1\Delta_g)$  mixing ratio at 60 km as a function of time on January 24, 1993. Crosses indicate the retrieved mixing ratios at 60 km for a single (50-70 km) solution layer, with horizontal bar indicating the length of the observation. Each vertical bar indicates the rms sum of uncertainties of the derived value. The solid curve represents the standard photochemical model  $O_2(^1\Delta_g)$  behavior. The dashed curve indicates the photochemical model result in the case where  $k(^1\Delta_g + O_2) \rightarrow O_2 + O(^1D)$  is reduced 40% below the JPL94 value.

**Figure 8.** Diurnal behavior of  $O_2(^1\Delta_g)$  at 60 km as a function of time on November 29 and 30, 1993. Crosses indicate the retrieved mixing ratios at 60 km for a single (50-70 km) solution layer, with horizontal bar indicating the length of the observation. Each vertical bar indicates the rms sum of uncertainties of the derived value. The solid curve represents the standard photochemical model  $O_2(^1\Delta_g)$  behavior. The dashed curve indicates the photochemical model result in the case where  $k(^1\Delta_g + O_2) \rightarrow O_2 + O(^1D)$  is reduced 40% below the JPL94 value.

**Figure 9.** Diurnal behavior of  $O_3$ . Crosses indicate the retrieved mixing ratios at 52 km for a two layer (48-58 and 58-72 km) fit to the observations, with horizontal bar indicating the length of the observation (6-12 minutes) and vertical bar indicating the uncertainty of the derived value. Error bars are dominated by pressure broadening uncertainty. The solid curve represents the standard photochemical model  $O_3$  behavior. The dotted curve indicates the photochemical model result in the case where  $k(\text{HO}_2 + \text{O}) \gg \text{OH} + \text{O}_2$  is reduced 40% below the JPL94 value. The 4-year zonal monthly mean values determined from SM $^2$  UV and  $\lambda$  (1.27 micron) observations are shown at the mid to late afternoon time period those observations were made.

**Figure 10.** Same as figure 9 for 60 km.

**Figure 11** Same as figure 9 for 68 km

**Figure 12.** Altitude profiles of the  $O_2(^1\Delta_g)$  1.27 micron volume emission rate. Values determined from SMF observations made on March 1983, are adopted from figure 8 of *Thomas et al.* (1984) Diamonds and triangles indicate the SMF results at 44°N and 0°N latitude, respectively, bracketing the 32°N latitude of Mt. Peak. Volume emission rates corresponding to our 2 mm observations are simply  $[O_2(^1\Delta_g)] \times A$ , and are shown by the solid and dotted curves for the Einstein A values  $2.6 \times 10^{-4}$  *Badger et al.*, 1965] and  $.5 \times 10^{-4}$  [*Mlynczak and Nesbitt*, 1995], respectively, with one solid and one dotted curve for each observation date. Error bars on the solid and dotted curves correspond to the uncertainties in  $O_2(^1\Delta_g)$  abundances derived from the 2 mm observations. Altitude profiles with one error bar represent one-layer (January and April, 1992) retrievals. Altitude profiles with two error bars represent two-layer (January and November, 1993) retrievals.

# Table

	Reaction
J <sub>1</sub>	$O_3 + h\nu \rightarrow O_2(^1\Delta_g) + O(^1D)$
k <sub>2</sub>	$O(^1D) + O_2 \rightarrow O(^3P) + O_2(^1\Sigma)$
k <sub>3a</sub>	$O_2(^1\Sigma) + N_2 \rightarrow O_2(^1\Delta_g) + N_2$
k <sub>3b</sub>	$O_2(^1\Sigma) + CO_2 \rightarrow O_2(^1\Delta_g) + CO_2$
k <sub>3c</sub>	$O_2(^1\Sigma) + O_3 \rightarrow O_2(^1\Delta_g) + O_3$
k <sub>3d</sub>	$O_2(^1\Sigma) + O \rightarrow O_2(^1\Delta_g) + O$
k <sub>3e</sub>	$O_2(^1\Sigma) + O_2 \rightarrow O_2(^1\Delta_g) + O_2$
k <sub>4</sub>	$O(^1D) + N_2 \rightarrow O(^3P) + N_2$
J <sub>5</sub>	$O_2 + h\nu(762nm) \rightarrow O_2(^1\Sigma)$
A <sub>6</sub>	$O_2(^1\Delta_g) \rightarrow O_2 + h\nu(1.27\mu m)$
k <sub>7</sub>	$O_2(^1\Delta_g) + O_2 \rightarrow O_2 + O_2$
k <sub>8</sub>	$O_2(^1\Delta_g) + N_2 \rightarrow O_2 + N_2$
k <sub>9</sub>	$O_2(^1\Delta_g) + O \rightarrow O_2 + O$
k <sub>10</sub>	$O(^1D) + O_2 \rightarrow O(^3P) + O_2$
A <sub>11</sub>	$O_2(^1\Sigma) \rightarrow O_2 + h\nu(762nm)$
J <sub>15a</sub>	$O_2 + h\nu \rightarrow O(^3P) + O(^1D)$
J <sub>15b</sub>	$O_2 + h\nu \rightarrow O(^3P) + O(^1D)$

Table 2

Error <b>Soil</b> cc	$\delta O_3$	$\delta O_2(\Delta_g)$	$\delta H_2O$
coll. width	15%	8%	18%
cali oration	5%	5%	5%
temperature	2%	0%	0%
spectral noise	~2%	2-8%	10-20%
RMS Total:	16%	10-12%	21-27%

# Table 3

Date	Elevation	Integration Time (hrs)	T <sub>sys</sub>	[O <sub>2</sub> ( $\Delta\epsilon$ )] <sub>obs</sub> /[O <sub>2</sub> ( $\Delta\epsilon$ )] <sub>model</sub>
Jan. 19+21, 1992	30°	7.0	3340	1.09±10%
Apr. 10, 1992	20°	1.0	2100	1.31±10%
Jan. 24, 1993	20°	2.0	1150	1.03±10%
Nov. 29+30, 1993	20°	6.8	1760	1.26±10%

Table 4

	Jan 1992	Apr 1992	Jan 1993	Nov 1993
Kitik Peak:				
Num. Obs.	2	1	5	2
[O <sub>3</sub> ] <sub>@ 55 km (ppmv)</sub>	.50 ± 0.26	.70 ± 0.29	1.71 ± 0.29	1.44 ± 0.24
[O <sub>3</sub> ] <sub>@ 65 km (ppmv)</sub>	0.34 ± 0.058	0.50 ± 0.085	0.54 ± 0.092	0.33 ± 0.057
SME-IR:				
[O <sub>3</sub> ] <sub>@ 55 km (ppmv)</sub>	1.65	1.46	1.65	1.59
[O <sub>3</sub> ] <sub>@ 65 km (ppmv)</sub>	0.474	0.508	0.474	0.401
SME-UV:				
[O <sub>3</sub> ] <sub>@ 55 km (ppmv)</sub>	1.72	1.70	1.72	1.73
[O <sub>3</sub> ] <sub>@ 65 km (ppmv)</sub>	0.419	0.505	0.419	0.412
Model, JP1,94:				
[O <sub>3</sub> ] <sub>obs</sub> /[O <sub>3</sub> ] <sub>model</sub> <sub>@ 55 km</sub>	1.12	1.18	1.21	1.04
[O <sub>3</sub> ] <sub>obs</sub> /[O <sub>3</sub> ] <sub>model</sub> <sub>@ 65 km</sub>	0.896	1.17	1.41	0.889
Model, k(H <sub>2</sub> O <sub>2</sub> + O) = 0.6 × k <sub>JP1,94</sub> :				
[O <sub>3</sub> ] <sub>obs</sub> /[O <sub>3</sub> ] <sub>model</sub> <sub>@ 55 km</sub>	0.943	0.994	1.02	0.883
[O <sub>3</sub> ] <sub>obs</sub> /[O <sub>3</sub> ] <sub>model</sub> <sub>@ 65 km</sub>	0.740	0.926	1.16	0.740

Table 5

	<i>Jail</i> 1992	Apr 1992	Jan 1993	Nov 1993
Kitt Peak:				
[H <sub>2</sub> O]@ 55 km (ppmv)	6.5± <b>1.6</b>	6.9±1.5	5.5± <b>1.2</b>	6.4±1.7
[H <sub>2</sub> O]@ 65 km (ppmv)	6.3± <b>1.5</b>	5.8±1.5	5.1±1.2	4.8±1.2
Table Mt.:				
[H <sub>2</sub> O]@ 55 km (ppmv)	6.1	7.1	6.1	6.0
[H <sub>2</sub> O]@ 65 km (ppmv)	5.1	5.4	5.0	6.0
UARS MLS:				
[H <sub>2</sub> O]@ 55 km (ppmv)	6.2±1.4	6.9±1.6	6.7±1.5	-

Fig 1: 255GHz  $O_2(^1\Delta)$ , 10 Apr92, 1:30–2:30 pm

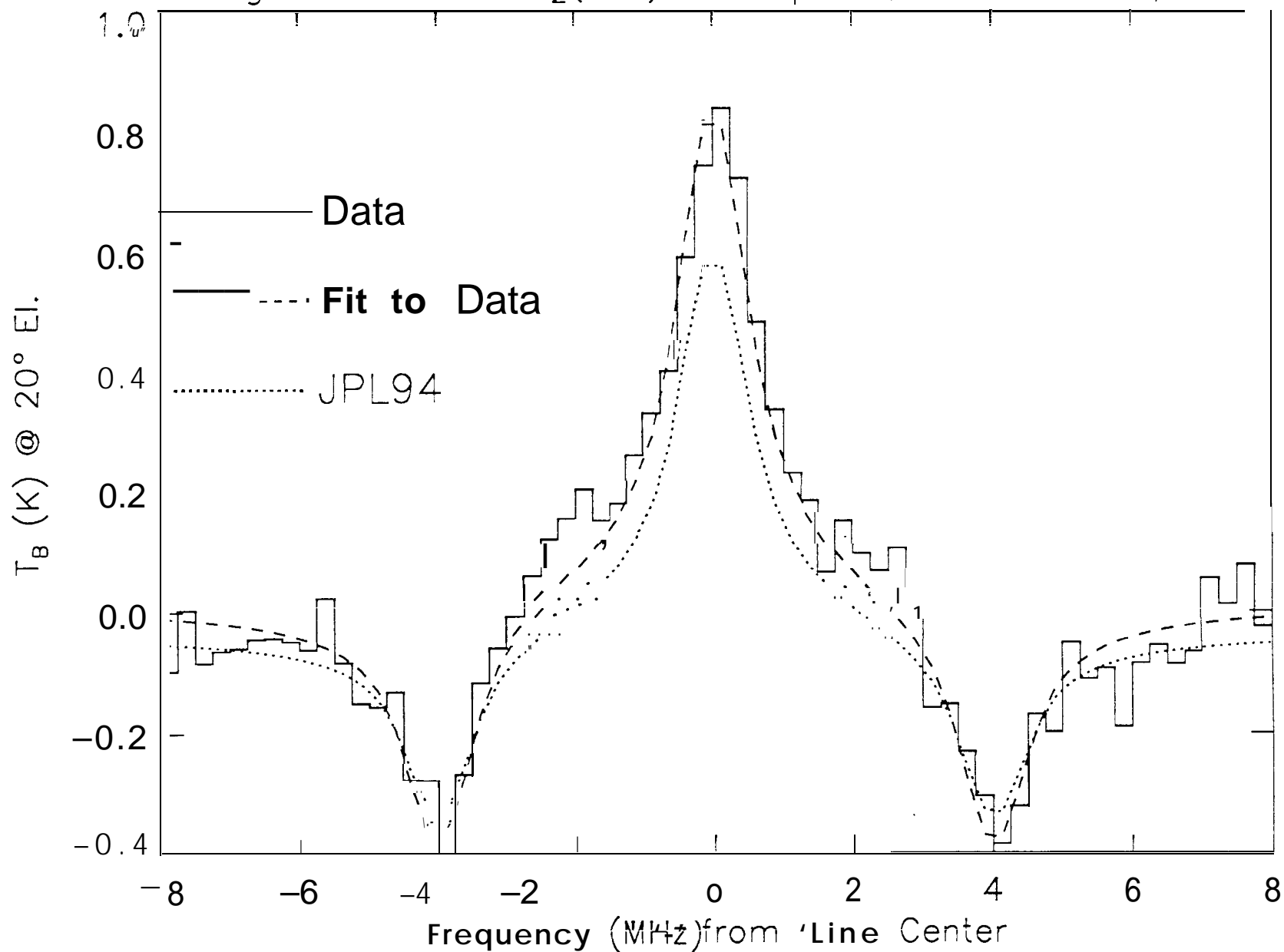


Fig. 2: 249 GHz O<sub>3</sub>, 10 Apr92, 1:00pm

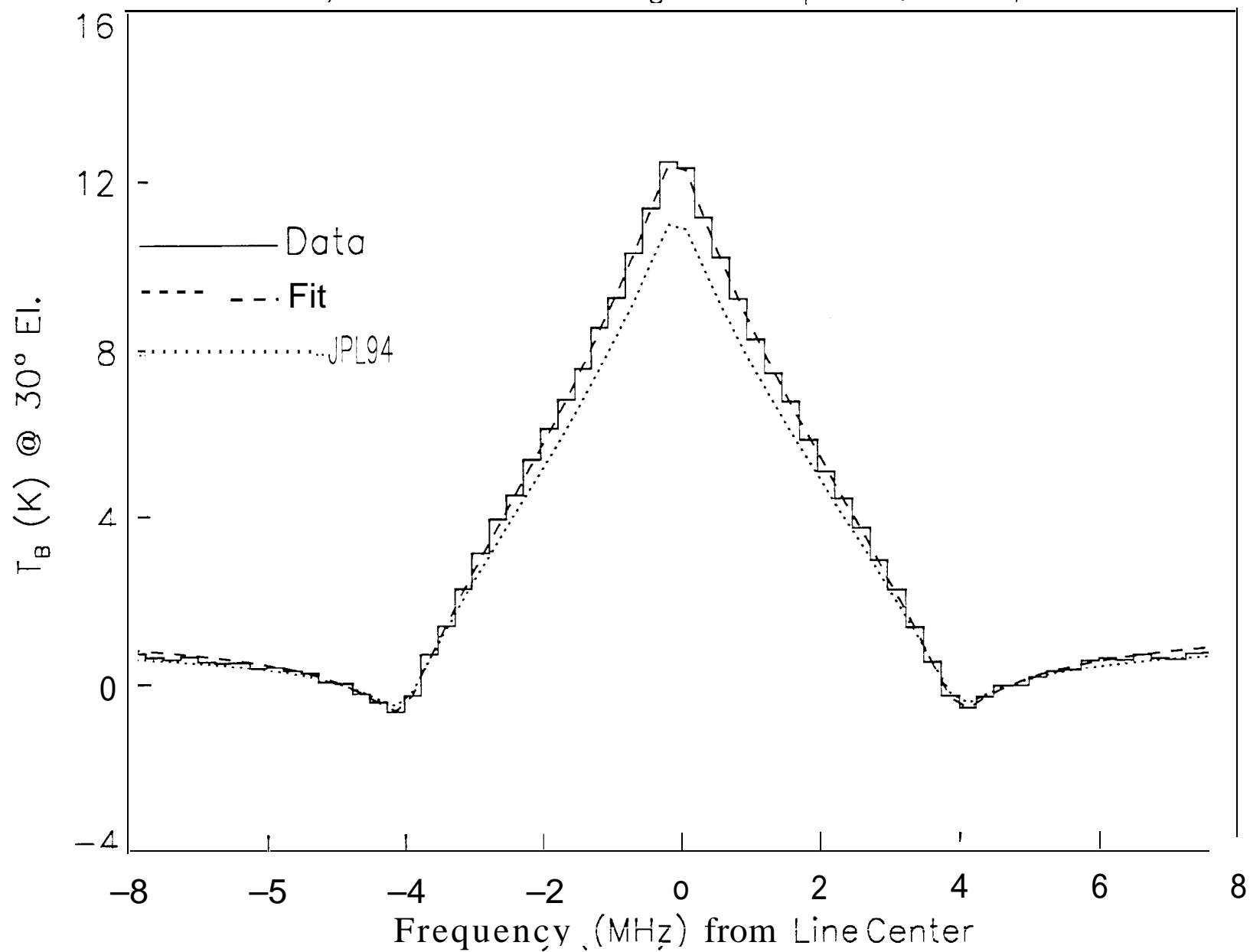


Fig. 3: 203GHz H<sub>2</sub><sup>18</sup>O, 10Apr92

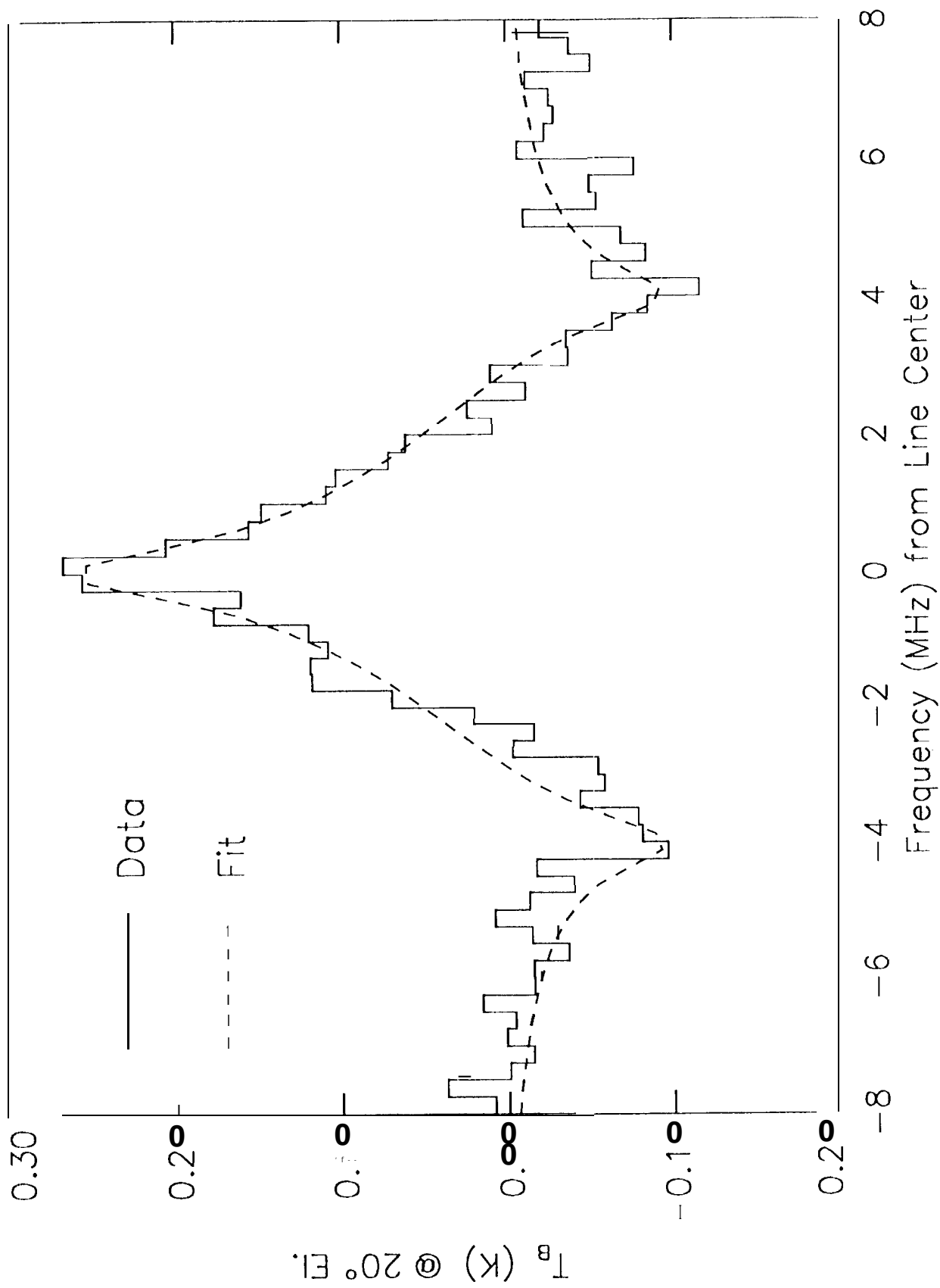


Fig. 4: Observed  $O_2(^1\Delta_g)$

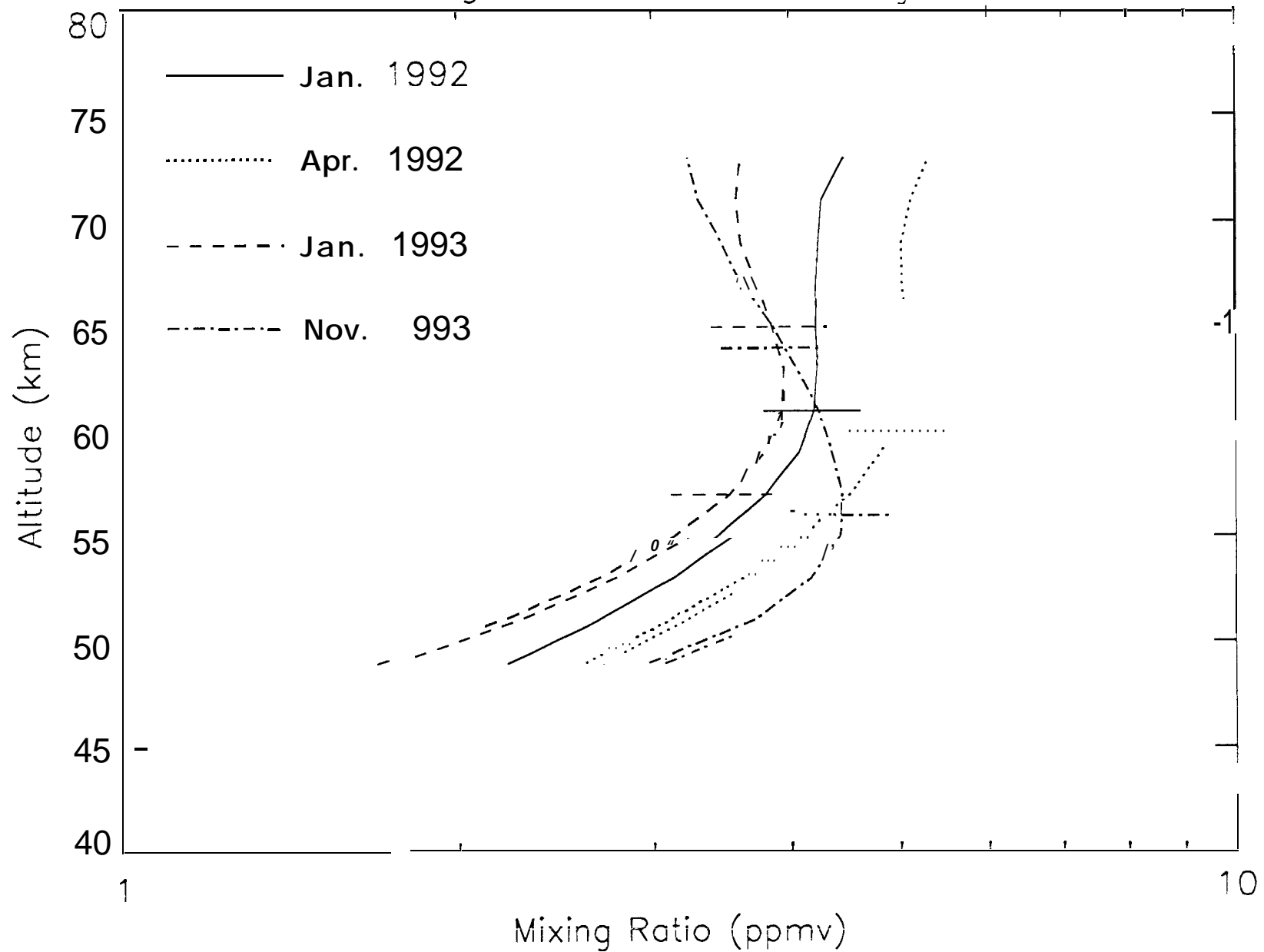


Fig. 5: Observed H<sub>2</sub>O

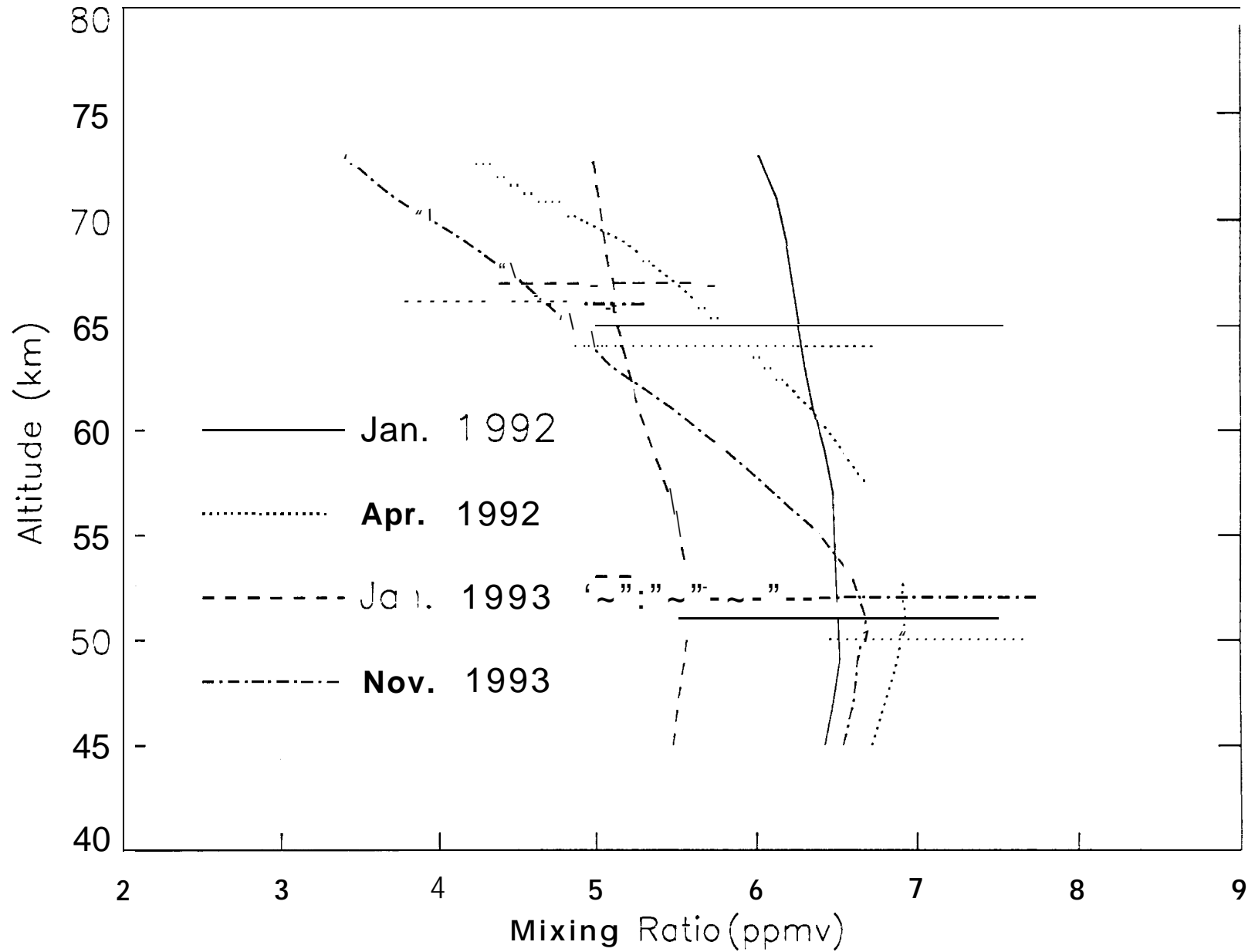


Fig. 6: 10Apr92 O<sub>3</sub> 1:00pm

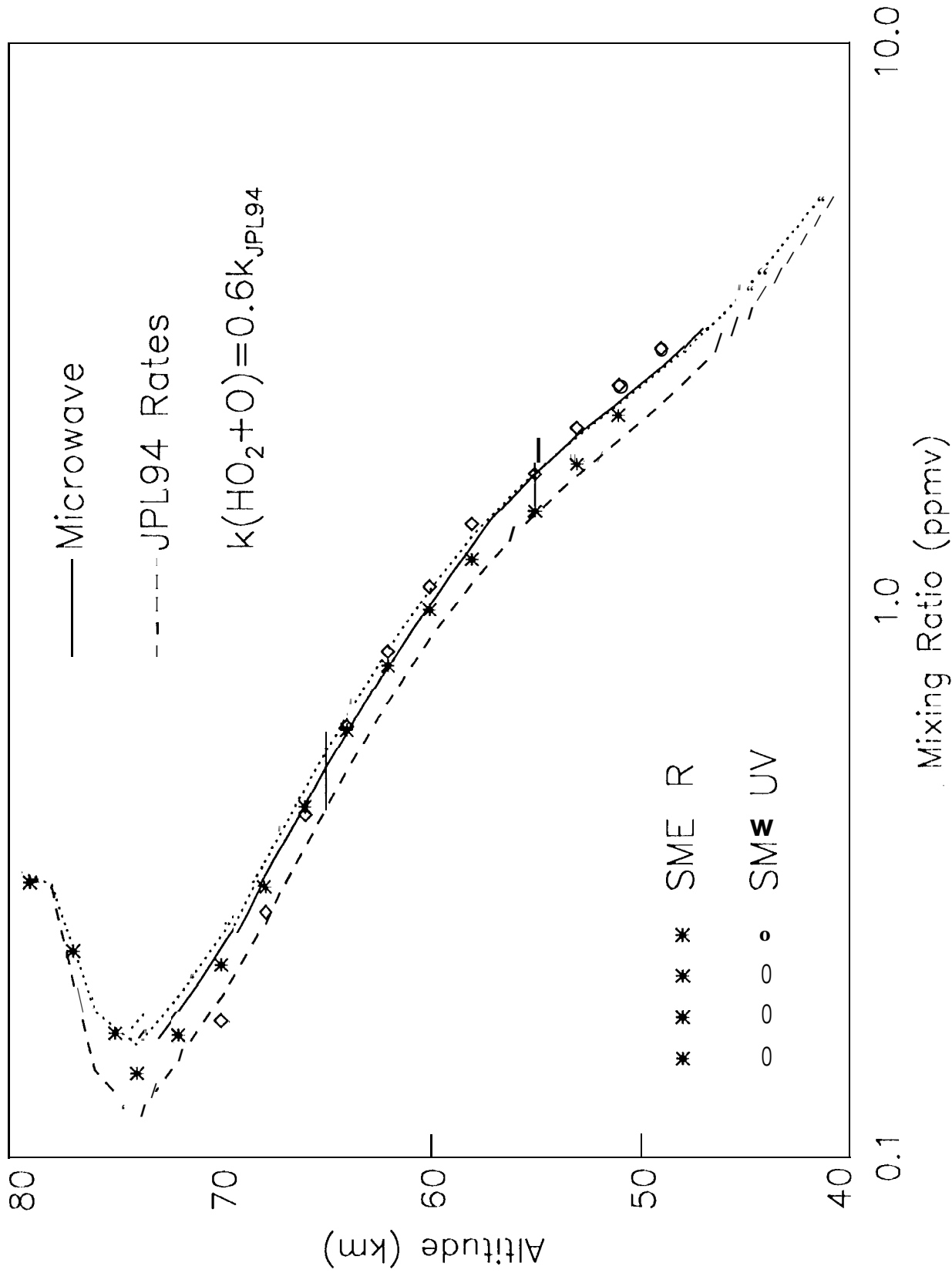


Fig 7: 24Jan93 O<sub>2</sub>(<sup>1</sup>Δ<sub>g</sub>) 60 km

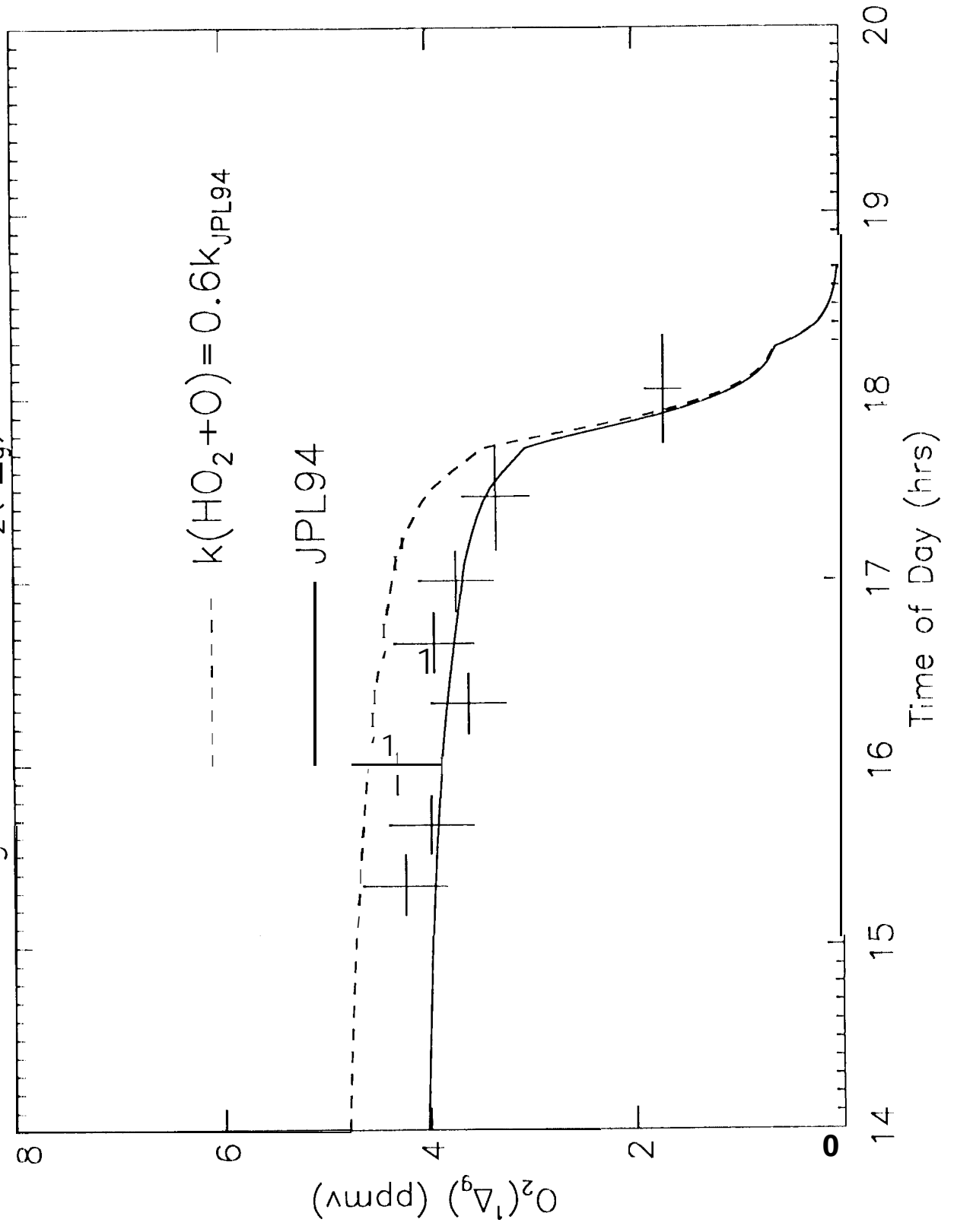


Fig 8: Nov93  $O_2(^1\Delta_g)$  (60 km)

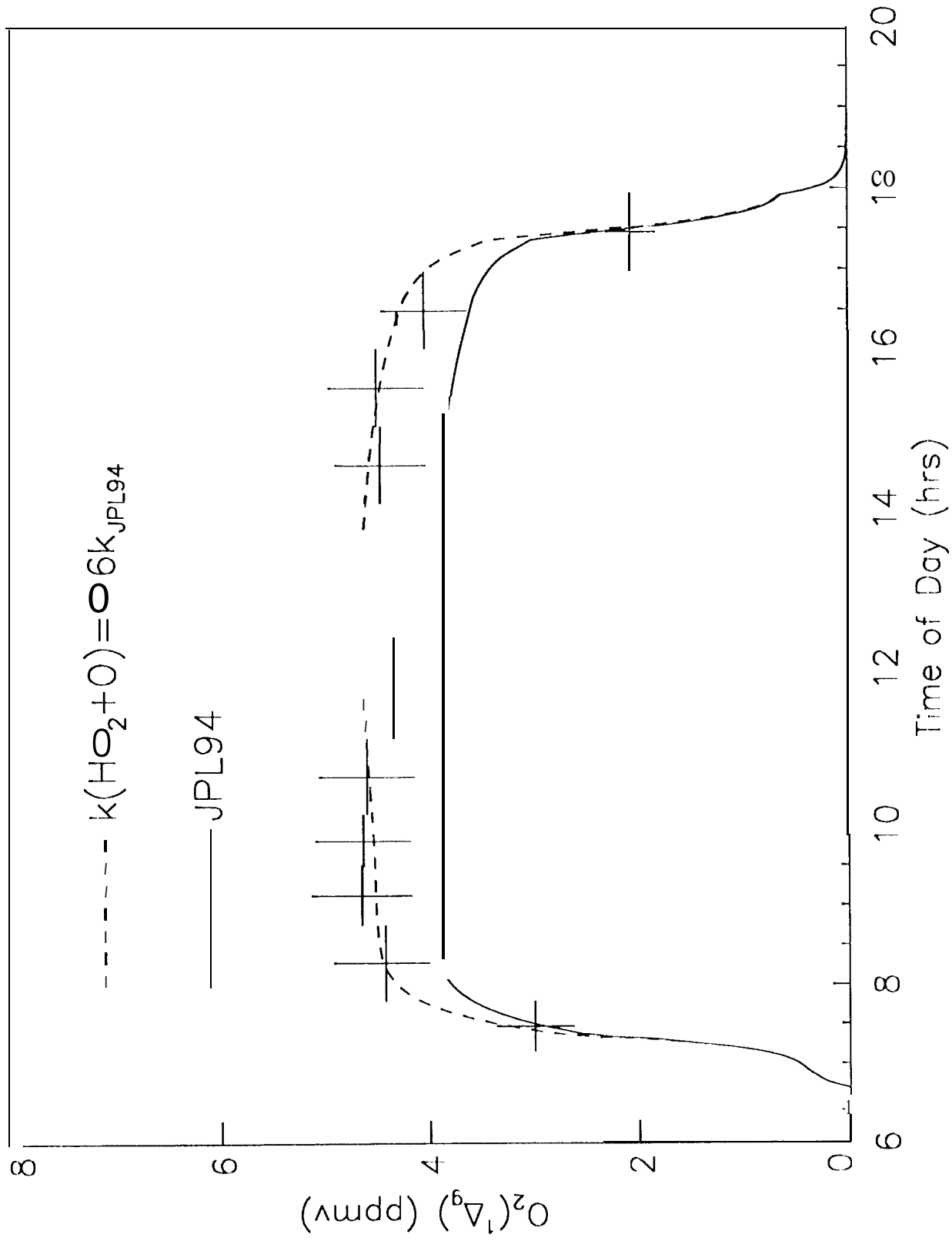


Fig 9: 23-25Jan93  $O_3$ , 52 km

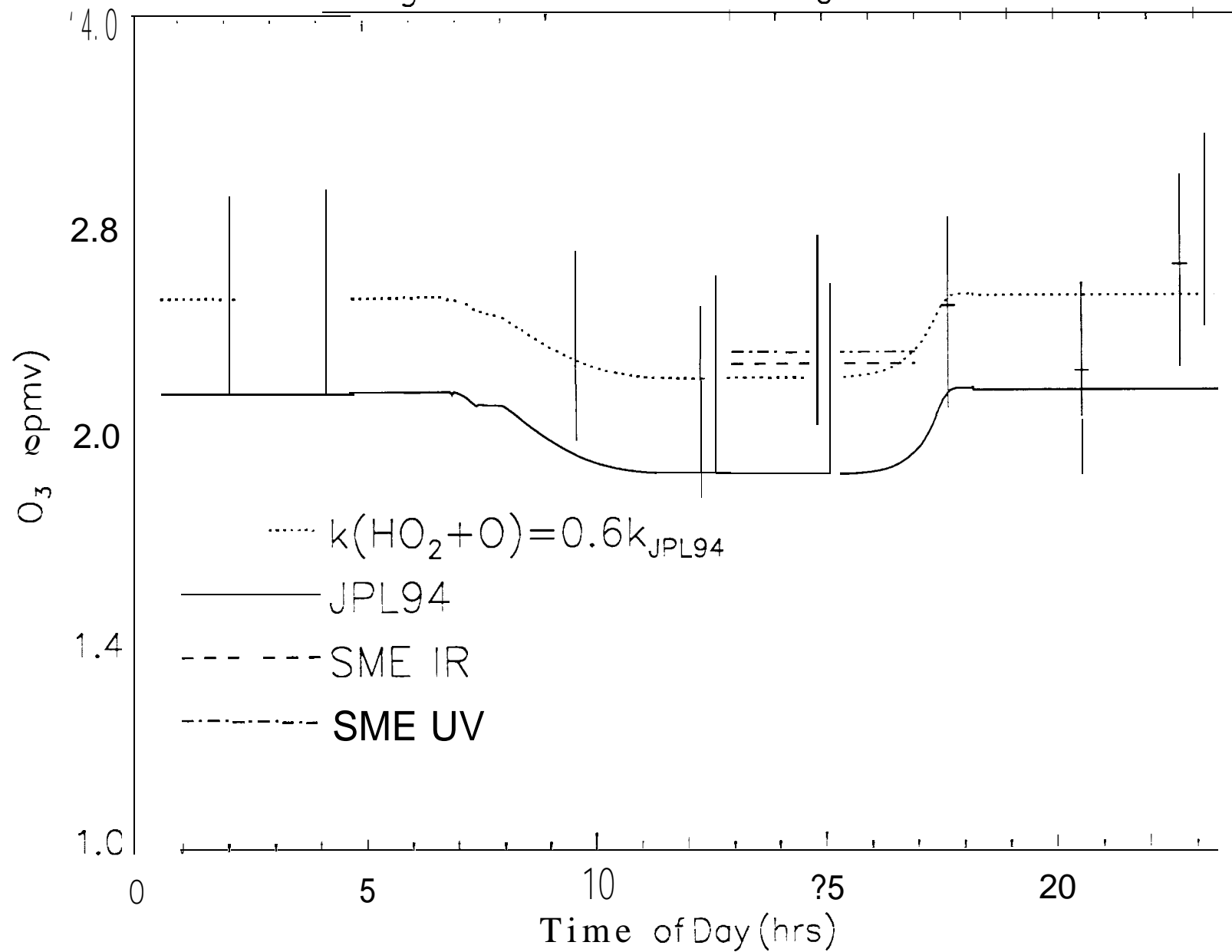


Fig 10: 23-25Jan93 O<sub>3</sub>, 60 km

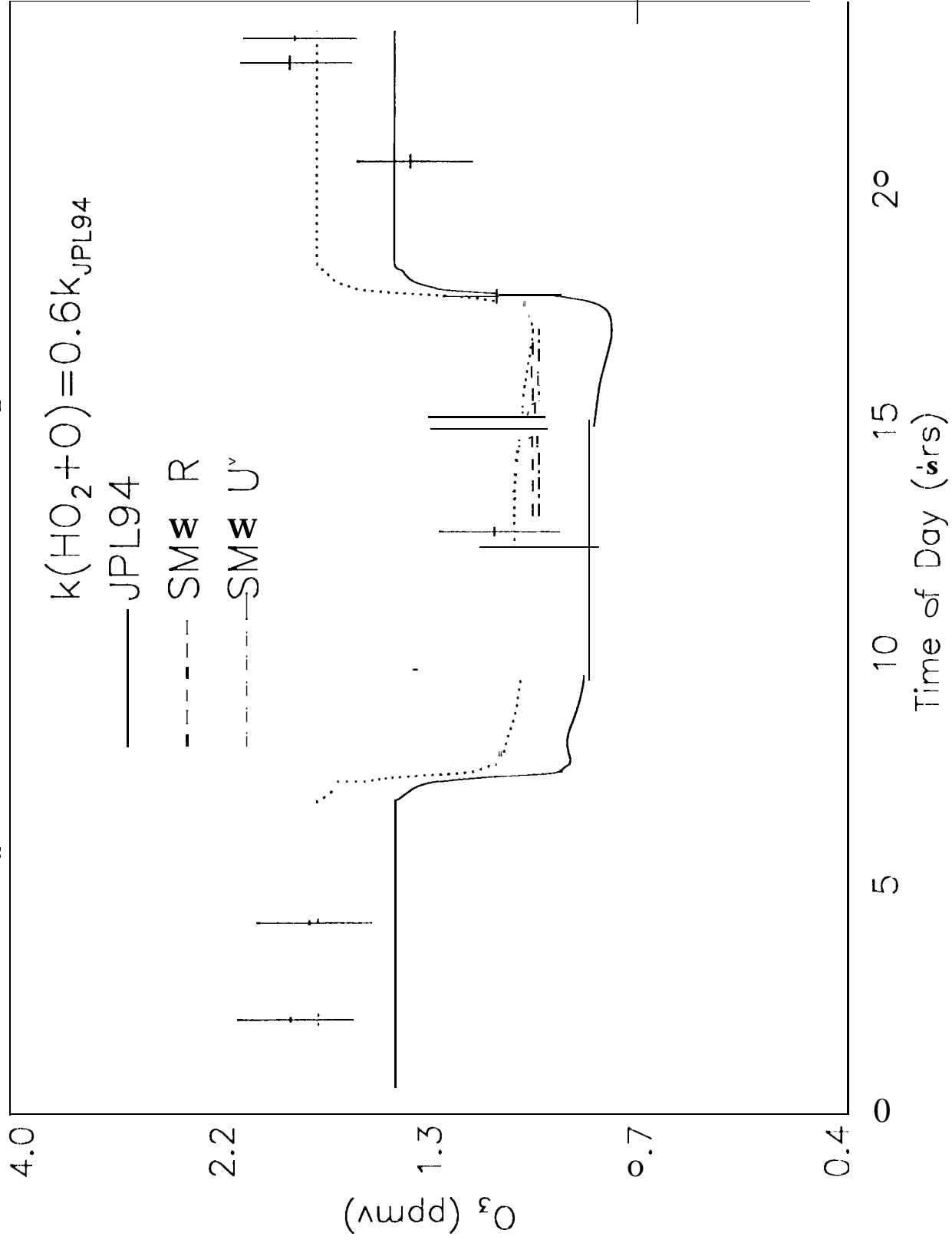


Fig 11: 23-25Jan93 O<sub>3</sub>, 68 km

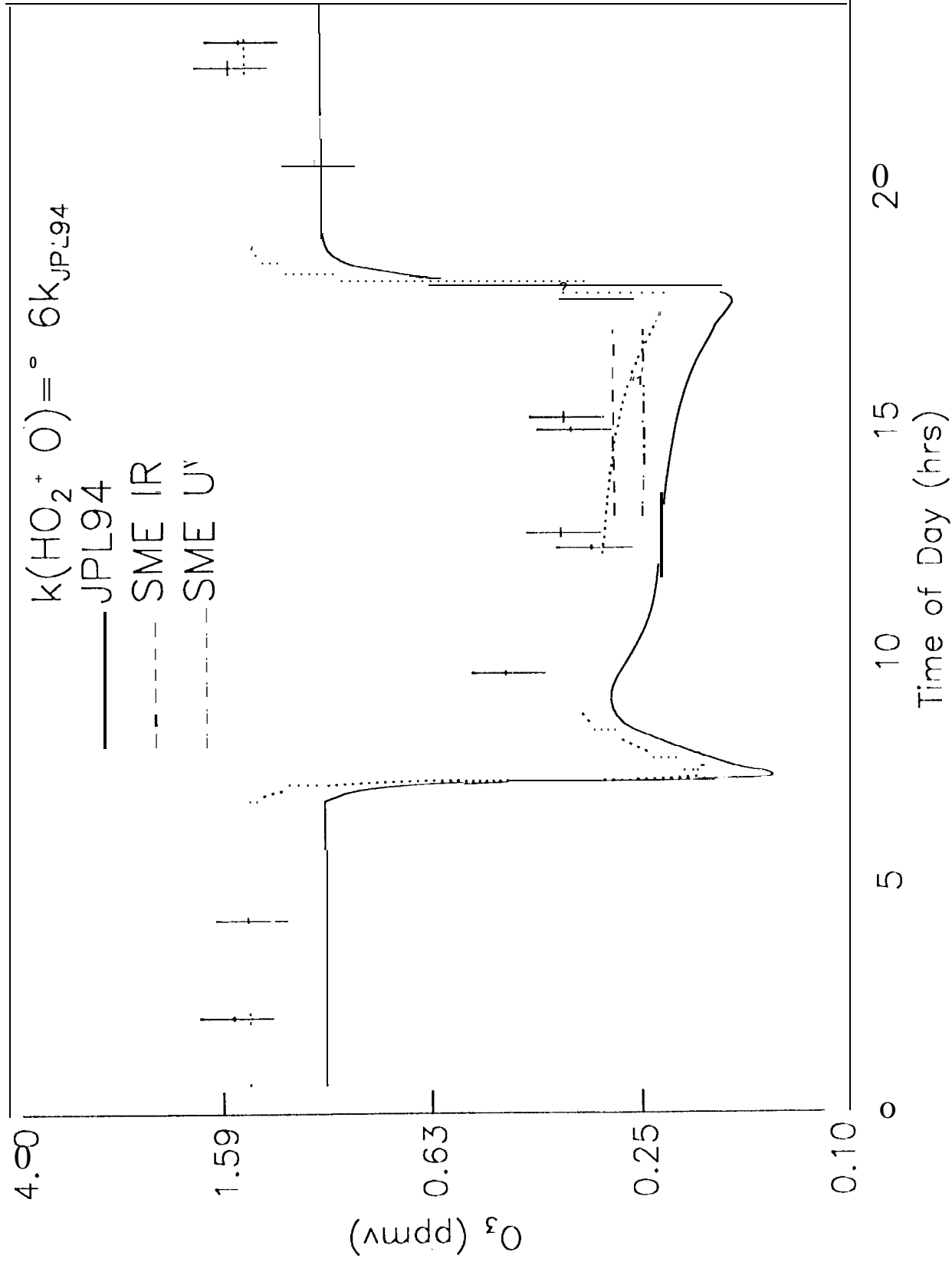


Fig 12: 1.27  $\mu\text{m}$  Emission

